Int. J. Heat Mass Transfer. Vol. 34, No. 7, pp. 1695–1706, 1991
Printed in Great Britain

0017–9310/91 $3.00 + 0.00

Convective boiling in a rod bundle: transverse variation of vapor superheat temperature under stabilized post-CHF conditions

C. UNAL,† K. TUZLA, O. BADR,‡ S. NETI and J. C. CHEN
Institute of Thermo-Fluid Engineering and Science, Lehigh University, Bethlehem, PA 18015, U.S.A.

(*Received* 29 *November* 1989 *and in final form* 8 *August* 1990)

Abstract—Transverse variations of vapor superheat temperatures across a rod bundle are measured for convective boiling of water in the post-CHF regime. Significant differences in superheat (up to 120°C) are observed across the flow subchannels. The steepness of this transverse superheat profile decreases with increasing vapor Reynolds number.

INTRODUCTION

IN BOILING heat transfer systems, critical heat flux (CHF) occurs when the heated surface can no longer support continuous liquid contact. These systems normally operate in the nucleate boiling regime where high heat fluxes may be obtained at relatively low superheat temperatures of the heating surface. However, boiling in the post-CHF regime can lead to high superheat temperatures at the wall surface. Accurate prediction of the surface temperature requires knowledge of the post-CHF heat transfer process.

Heat transfer in the post-CHF regime has often been modeled with the assumption of thermodynamic equilibrium between the liquid and vapor phases. More recent models have attempted to consider the possible existence of thermodynamic nonequilibrium, where superheated vapor would coexist with entrained liquid droplets. Measurement of this nonequilibrium phenomenon in rod bundles is the primary purpose of the present work.

Though a number of convective film boiling experiments have been conducted over the past 20 years, only a few attempts to quantify the degree of thermodynamic nonequilibrium have been reported. Mueller [1] and Polomik [2] obtained some limited data at high vapor qualities for internal flow in a tube. Hochreiter [3] obtained some indication of vapor superheats in rod bundles limited primarily to high vapor quality conditions (see also Loftus *et al.* [4]). Nijhawan *et al.* [5] successfully used an aspirated thermocouple probe to obtain measurements of vapor superheats at one axial location for convective film boiling in a tube. Gottula *et al.* [6] and Swinnerton *et al.* [7] extended the tube data to higher mass fluxes and higher pressures. Evans *et al.* [8] extended the available data with slow moving quench front experiments in a vertical tube.

Recently, as a part of the present study, post-CHF data were obtained [9–11], with vapor superheat measurements, in a rod bundle geometry. All of the above studies [5–11] measured the non-equilibrium vapor temperature at a single transverse position of the flow channel. Their emphasis was on the *axial* variation of vapor superheat in post-CHF convective boiling. To date, there is no published data on the transverse variation of vapor superheat across the flow channel.

In a typical post-CHF heat transfer experiment, the dependent parameters to be measured include the vapor temperature, the wall temperature and the wall heat flux. In these experiments, it is desirable to hold the quench front (CHF) at a fixed location in the test section in order to: (i) maintain steady-state conditions in the test section, (ii) permit easier measurement of the desired parameters, (iii) obtain vapor temperature measurements at a fixed and well-established distance from the CHF location, and (iv) allow to traverse the vapor probe across the channel to obtain data on transverse variation of vapor superheat. However, arresting the quench front at a fixed location in a rod bundle represents a major operating difficulty.

Groeneveld and Gardiner [12] were the first to obtain steady-state post-CHF flows in a test section using a large thermal mass (hot-patch) at the test section inlet. To generate the post-CHF conditions, the test section and hot-patch were preheated to temperatures well above the Liedenfrost wetting temperature (approximately 500°C for water at atmospheric pressures), before introduction of the two-phase flow. High thermal mass of the hot-patch delayed the quench front propagation, giving an opportunity to adjust the power input to the test sec-

† Present address: Los Alamos National Laboratory, Los Alamos, NM 87545, U.S.A.
‡ Present address: UAE University, United Arab Emirates.

NOMENCLATURE

C_p	specific heat [kJ kg^{-1} °C^{-1}]
D	diameter [m]
G	mass flux [kg m^{-2} s^{-1}]
P	pressure [kPa]
q	heat flux [W m^{-2}]
R	radius [m]
Re	Reynolds number [—]
T	temperature [°C]
X	vapor mass quality [kg kg^{-1}]
Y	transverse distance [m].

Greek symbol

μ	viscosity [kg m^{-1} s^{-1}].

Subscripts

a	actual
c	center of the flow channel
CHF	critical heat flux
e	equilibrium
hr	hot-rod
HP	hot-patch
in	inlet to hot-patch
int	inlet to test section
r	rod
s	saturation
v	vapor
w	wall.

tion to arrest the progress of the quench front and to maintain steady post-CHF conditions. Such steady-state post-CHF conditions have been achieved also by Nijhawan *et al.* [5], Gottula *et al.* [6], Swinnerton *et al.* [7] and Evans *et al.* [8] for single tube experiments.

In the present experiments, the hot-patch technique was applied to a rod bundle geometry for the first time. The post-CHF facility required several unique experimental developments, as described elsewhere [13, 14]. Successful operation resulted in measurements of superheated vapor temperature profiles across the rod bundle, both upstream and downstream of a grid spacer. Data from such experiments will aid the development of more accurate post-CHF heat transfer models.

EXPERIMENTS

A recirculating flow boiling loop (see ref. [15] for more information) was used for the present work. Subcooled water was pumped by a pair of metering pumps to a vertical tube boiler which provides a two-phase mixture of a known quality to the test section. The two-phase mixture leaving the test section flowed to a separation tank. The water collected at the bottom of the separation tank flowed to a water-cooled condenser while the steam outlet at the top was controlled by a back pressure regulating valve. The condensate flowed back to the surge tank. Mass flow rate was measured at the downstream side of the metering pump, and fluid temperatures were measured at the boiler inlet and outlet, the test section inlet, and the condenser outlet for overall control of the flow loop.

Test section

The 3×3 rod bundle test section was designed to be representative of pressurized water reactors. The bundle, as shown in Fig. 1(a), consists of nine rods of 9.5 mm o.d., 12.6 mm pitch and surrounded by a square shroud.

A schematic diagram of the test section elevation is given in Fig. 1(b). The length of the actual test section (between points A and B) is 122 cm (48 in.). A spacer grid is used at 76.2 cm (30 in.) from the inlet (Point A) to allow the study of its effects on wall temperature, vapor temperature and other parameters. The two instrumentation ports which are located on one side of the shroud (port #2 and #3 in Fig. 1(b)) were used for vapor temperature and pressure measurements.

The test rods are similar in size to typical PWR fuel rods (9.5 mm o.d.) and are internally heated with uniform heat flux by using a high resistance ribbon embedded in boron nitrite. The heated length of the rods extends above the test section by 120 mm to prevent quenching the test section from the top, and extensions of test rods (150 mm) below the test section (called hot rods) are used as a part of the lower hot-patch. Each rod is equipped with 12 thermocouples placed in grooves to measure the wall temperature. An electrically heated tubular furnace with three independently controlled zones surrounding the shroud is used to heat the shroud. The required heat flux is obtained by controlling the temperature of the furnace refractory (up to 1200°C) relative to the shroud temperature. The shroud is made of a 2 mm thick sheet of Inconel 625 alloy and has 16 externally brazed type K thermocouples along the length to monitor its wall temperature. Additional details pertaining to the test section and the two-phase loop design are presented elsewhere [14, 15].

Hot-patch

Stabilized post-CHF data have been obtained by several researchers through the use of the hot-patch technique for single tube experiments. The geometry of the single tube permits the use of a large metal (copper) block, with high heat conductivity and high heat storage capability, so that it can supply the required high heat flux to the CHF location. In a rod bundle geometry, the problem is obviously more complicated, in that each individual rod requires a separate hot-patch with no major changes in flow

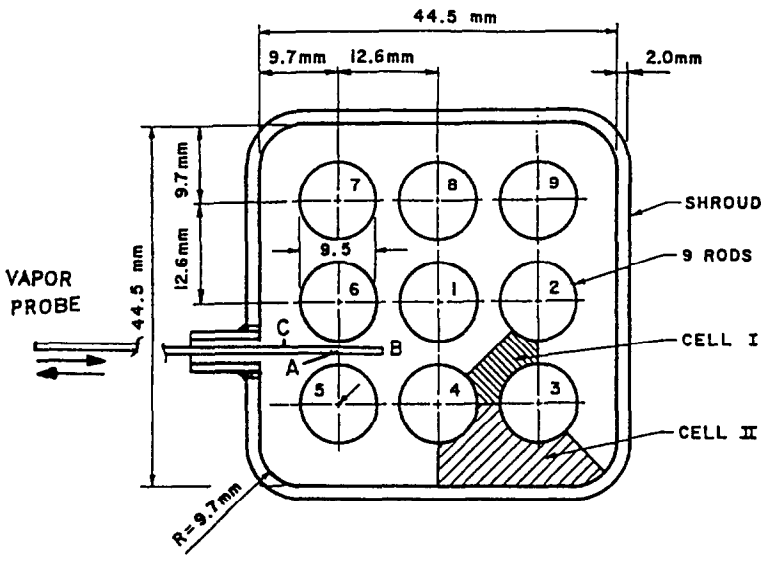

FIG. 1(a). Cross-sectional view of the test bundle.

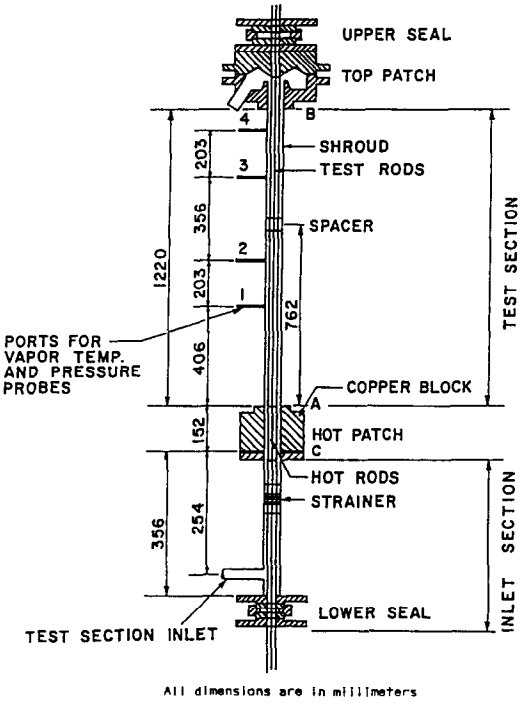

FIG. 1(b). Schematic diagram of the test bundle.

cross-sectional area. The internally heated high heat flux rods (hot-rods) with the same outside diameter as the bundle rods (test rods) were implemented as extensions toward the inlet. In order to test the feasibility of the hot-rod concept before fabrication, a sample rod was constructed and tested. The experiment consisted of a cartridge heater, 9.5 mm o.d. and 15 cm long, with a 1.5 mm thick copper oversleeve. The hot-rod was placed in a 25 mm i.d. tubular test section where it could be exposed to two-phase flows of various qualities and flow rates. A schematic of the test set-up is shown in Fig. 2 with the test results, indicating the required heat fluxes to stabilize the quench front for various inlet qualities. The hot-patch for the shroud is made of copper and is similar to that used with a single tube. A schematic of this lower hot-patch is shown in Fig. 3.

The upper end of the test section is also required to be kept at higher wall superheats, in order to prevent any quench propagation from the outlet of the test section. This is achieved by: (i) extending the test rod heaters beyond the test section length, and (ii) using a heated copper block at the upper end of the shroud (Fig. 4). The liquid and vapor exiting from the test section are collected in a plenum and discharged into the return pipe of the loop. To further reduce the heat losses from the plenum walls to the fluid, the plenum is covered with sheet metal, which is about 2.5 mm (0.1 in.) away from the plenum wall with a gap maintained in between.

The preliminary tests indicated the need for use of different heat fluxes for each hot rod, at least for short periods of time, although the long-term average powers could be the same for all of them. In order to provide variable heat fluxes to the hot-rods, a magnetic relay was installed in each hot-rod power line. The relays were operated on/off individually, depending on the surface temperature of the individual hot-rod in question. This was done with the use of an additional temperature controller for each hot-rod. With this hot-rod power control system, the hot-patch, hot-rod combination was able to arrest the quench front below the test section inlet for all the anticipated experimental conditions given below. A sample plot of the temperature histories of five hot-rods are shown in Fig. 5. Temperatures of the rods

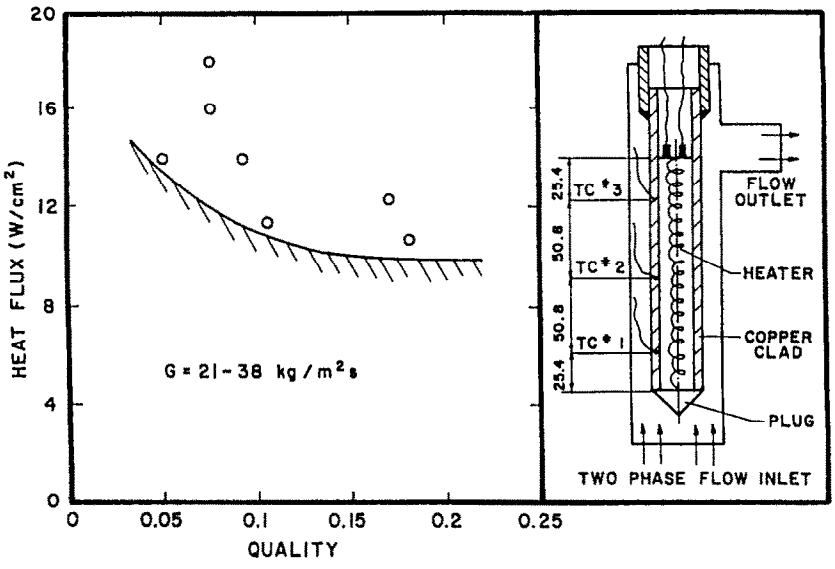

FIG. 2. Domain of stable quench front during single 'hot-rod' tests.

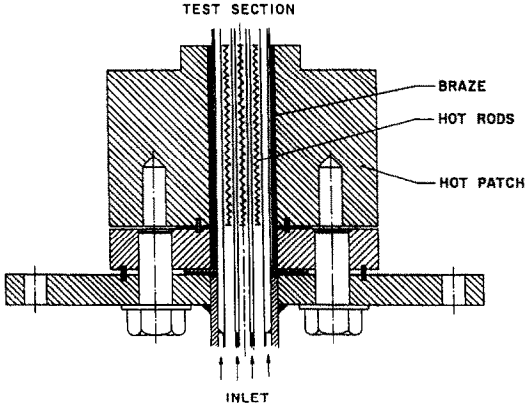

FIG. 3. Lower hot-patch assembly.

varied by $\pm 20°C$ with the opening and closing of the relays, but the mean values stayed constant. The small differences between the mean temperature values were due to minor differences between the individual temperature controllers.

Measurement of vapor superheat

The vapor superheat probe used in the present rod bundle experiments is similar in concept to those developed by Nijhawan *et al.* [5] and used by Evans *et al.* [8] and Gottula *et al.* [6]. As shown in Fig. 6, it utilizes two shields on a thermocouple for: (a) the inertial separation of liquid droplets from the sampled vapor, (b) the differential aspiration of the separated phases to minimize probe quench by liquid, and (c) multiple radiation shielding of the thermocouple junction to minimize radiation heat transfer from the neighboring hot walls. The probe consists of a 2.13 mm diameter 304 stainless steel outer tube and a 1.25 mm diameter 304 stainless steel inner tube as shown in Fig. 6. The rest of the plumbing accomplishes the appropriate aspirations. A 0.25 mm diameter grounded stainless stell sheathed type K thermocouple is used for the temperature measurement. The probe is movable in the lateral plane, into and out of subchannels, because of the bellows provided therein. The operation of the vapor probe is operator dependent and also a strong function of the vapor quality of the two-phase flow in the test section [8, 9].

Some results obtained with the vapor probe described above are shown in Figs. 7 and 8. The plots are time histories of the vapor temperature recorded on a strip chart and are classified according to the type of signal as ratings 1–4. The trace corresponding to rating 1 (Fig. 7) indicates very few droplets in the probe and thus the vapor temperature can be read right off the chart as the mean corresponding to the top of the line indicated. The dips in the temperature shown in rating 2 are indications of liquid droplets reaching the probe thermocouple and the complete recovery of the thermocouple to the vapor temperature (T_v) is evident. Figure 8 shows two types of traces (ratings 3 and 4) that result when larger amounts of liquid exist in and around the vapor probe. The estimated vapor temperatures corresponding to the two plots are also shown. When larger amounts of liquid phase exist in the vicinity of the probe (rating 4), the probe thermocouple has no opportunity to recover in the traditional sense, to display the asymptotic behavior shown in rating 2 of Fig. 7. In this case, the vapor superheat is interpreted to be in the range shown and at least as high as indicated by the lower peaks in the plot. All of the data presented in later sections of this paper had vapor temperature trace ratings of 1, for which the estimated experimental uncertainty was $\pm 7°C$. Furthermore, these vapor temperatures include additional uncertainties due to disturbance and mixing effects of the probe tip. Therefore, the vapor temperatures presented here should be

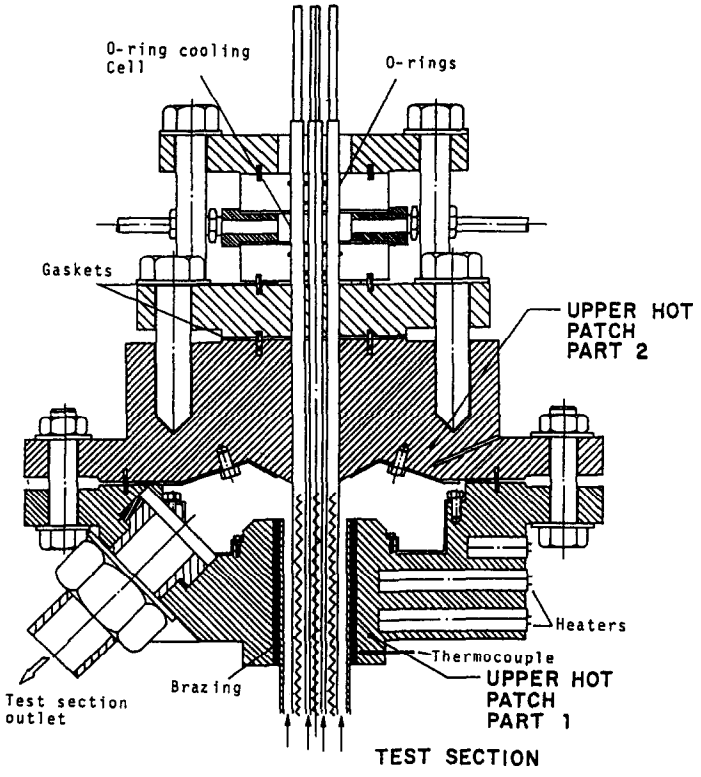

FIG. 4. Top-patch and upper sealing assembly.

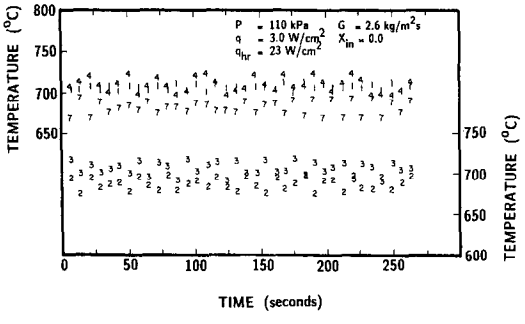

FIG. 5. Temperature histories of five hot-rods for a successful experiment.

considered as mean values over a finite cross-section that is equal to the projection area of the probe tip.

Insertion of the probe into the flow field could distort the flow and alter the wall and vapor temperatures as compared to the case without the probe insertion. This was experimentally checked, by observing wall temperature variation as the probe tip was traversing the channel. No significant temperature variation was observed on the wall while the probe was traversing the channel from point B to A as shown in Fig. 1(a).

Test procedure

In a typical stabilized post-CHF experiment, the test section would be preheated to a selected post-CHF state with the shroud, rods and hot-patch at substantial superheats. A steady two-phase flow, with desired flow rate, pressure, and inlet mixture enthalpy would be established, using a bypass around the test section during the preheating stage. Upon obtaining the desired initial condition, data acquisition was started and the two-phase fluid would be switched from the bypass line to the test section. By proper adjustment of the hot-patch and hot-rod power, the dryout quench front would be arrested at the inlet of the hot-patch, providing stabilized post-CHF conditions in the test section (see refs. [9–11]). A total of 74 and 62 data sets were recorded for the upstream and downstream vapor probes, respectively. The vapor superheat data included the following range of flow parameters:

mass flux:	7–26 kg m^{-2} s^{-1}
pressure:	105–120 kPa
inlet vapor quality:	40°C subcooled to 0.40
heat flux:	19.1–43.0 kW m^{-2}.

RESULTS AND DISCUSSION

Sample results

The primary information recorded was spatially varying temperatures of two-phase vapor and the heater rods. Figure 9 shows a representative plot of the rod and vapor temperatures measured along the length of the test section. The open circles represent surface temperatures measured on the nine rods in the test section at the various elevations indicated. The uniformity and smoothness of this composite curve confirms the similarities of thermal-hydraulic con-

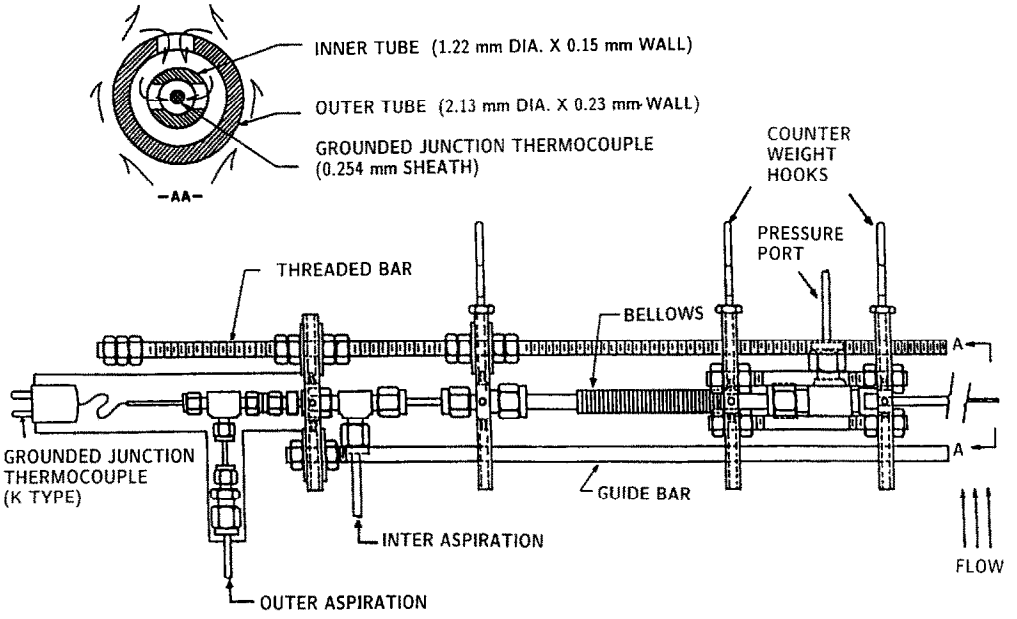

FIG. 6. Schematic of the traversable miniature vapor superheat probe.

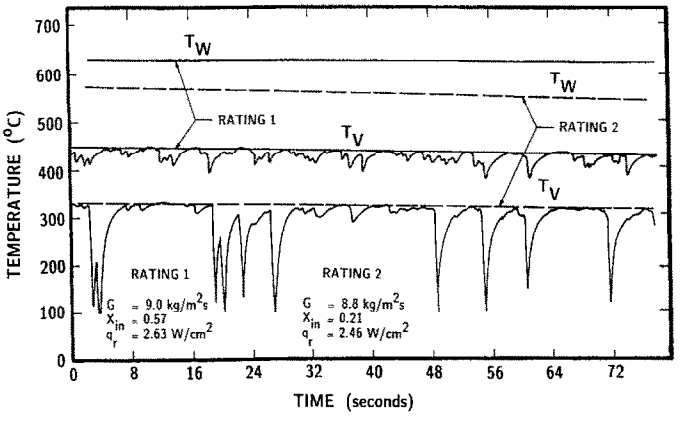

FIG. 7. Vapor superheat probe traces for higher vapor qualities.

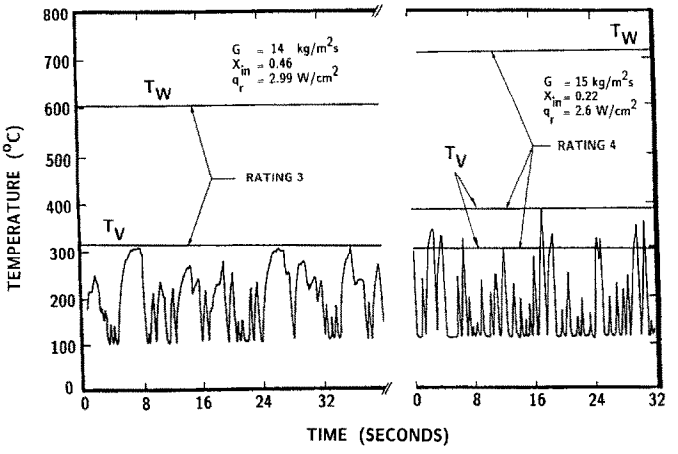

FIG. 8. Vapor superheat probe traces for lower vapor qualities.

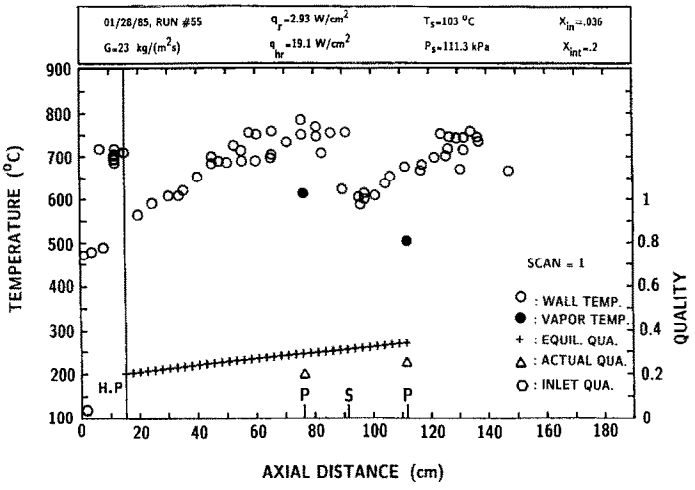

FIG. 9. Variation of wall and vapor temperatures, and equilibrium and actual qualities with axial distance for a sample fixed-CHF run.

ditions in all flow subchannels of the rod bundle. Downstream of the CHF, the rod's surface temperature increases with a fairly uniform rate until the grid spacer. At the grid spacer, as indicated by the symbol S in Fig. 9, the rods experienced a sharp decrease in wall superheat, requiring an axial distance of approximately 0.2 m before recovering to the pre-spacer temperatures. This desuperheating effect of the grid spacer was consistently found in all experiments, indicating the promotion of enhanced two-phase cooling by the spacer obstruction. Axial locations of the two vapor probe stations are indicated by the symbol P in Fig. 9. During this particular experiment, the measurement tips of the vapor probes were located at the center of the inner cell (i.e. point B in Fig. 1(a)). These 'center-line' vapor temperatures are indicated by the dark symbols in Fig. 9. It is seen that the vapor attains a very significant level of superheat (500°C) at the upstream vapor probe location, and across the spacer the vapor temperature drops due to the desuperheating effects of the grid spacer on the two-phase fluid. More detailed information on the axial variation of vapor superheat can be found in ref. [11].

Due to the extreme difficulty of arresting the quench front at the beginning of the rod bundle, most of the available post-CHF data had been obtained by allowing the quench front to propagate upward to the test bundle. Post-CHF heat transfer data obtained from such a transient run, however, were never compared with the data obtained under stabilized post-CHF conditions to verify the agreement in wall and vapor temperatures for both types of runs. Comparison of a steady-state test from the present work with a previously obtained slow moving-CHF test [11] under similar flow conditions is of interest here. Matching the mass flux, wall heat flux, and equilibrium quality along the test section length beyond the hot-patch were the basis for this comparison. The wall and vapor temperatures and equilibrium qualities of moving-CHF and fixed-CHF runs are shown in Fig. 10 for almost the same mass flux of about 20 kg m^{-2} s^{-1}, and similar electrical wall heat fluxes. The equilibrium qualities at the test section inlet are 0.263 and 0.422 for the fixed-CHF and the moving-CHF runs, respectively. For the fixed-CHF runs, due to the high heat input in the hot-patch/hot-rod region, however, the equilibrium quality reaches a value of 0.49 at the hot-patch outlet, which is shown by the vertical solid line at a distance of 15.2 cm away from the origin. Thus equilibrium qualities at this location are also similar, 0.49 for the fixed-CHF test and 0.47 for the moving-CHF test. Similar equilibrium quality distributions are observed for the two runs for the rest of the test section. The wall temperatures shown in Fig. 10 belong to rods numbered 1, 2 and 3 in Fig. 1(a). It should be noted that distances between the quench front and the location of the vapor probe are relatively short in the moving-CHF test due to the absence of the hot-patch power in this run. The wall temperature profiles for the two runs are in good agreement except in the hot-patch region. In this immediate downstream region of the CHF, the initial sharp increase in the wall temperature, seen in the moving-CHF run, is compressed in a short distance in the fixed-CHF run. Furthermore, the hot-rods operate at relatively higher temperatures (about 700°C) to arrest the quench front. The wall temperatures right after the hot-patch outlet decrease to values expected to occur in the absence of the hot rods. At higher elevations, the wall temperatures are in good agreement, with an acceptable 10% scatter. Finally, the conclusion was that similar thermal-hydraulic conditions exist for fixed-CHF and slowly-propagating CHF tests, beyond the length of the hot-patch.

Transverse variation of vapor superheat

The first vapor probe was located at an axial distance of 762 mm downstream from the hot-patch inlet and 152 mm upstream of the grid spacer. The data

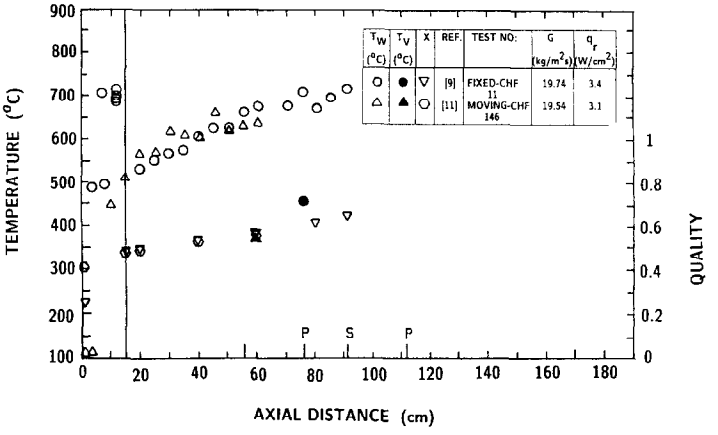

FIG. 10. Comparison of wall and vapor temperatures for similar fixed-CHF and moving-CHF runs.

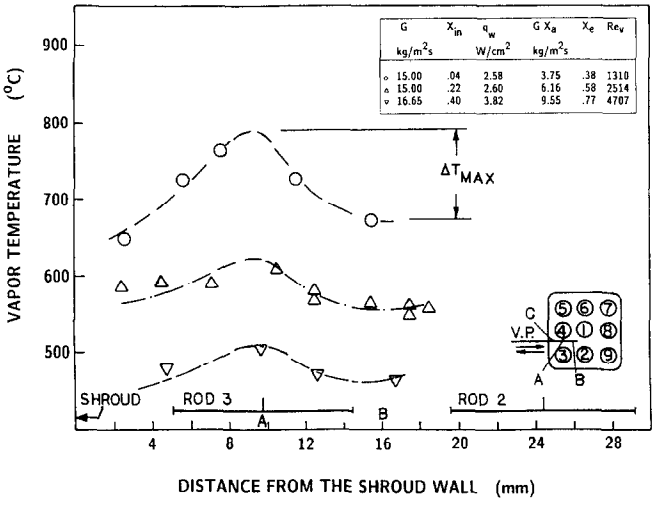

FIG. 11. Transverse vapor temperature profiles for various vapor qualities.

obtained from the first probe represents the transverse variation of vapor superheat in hydrodynamically established convective film boiling [16]. Typical transverse variations of vapor temperature for different inlet vapor qualities are shown in Fig. 11. The figure shows significant temperature differences, ΔT_{max} up to 120°C, in the cross-sectional plane of the test bundle, between points A and B in Fig. 11, for low inlet quality conditions. The profile has a bell shape with its maximum value obtained at the minimum channel width (point A), and its minimum values at the centers of inner and outer flow cells (points B and C). The symmetric behavior of the vapor temperature profile (between points A and B and points A and C), is, again, evidence of similar thermal-hydraulic conditions in the inner and outer cells. Also shown in Fig. 11 is the effect of inlet quality on the vapor temperature, as also reported elsewhere [9]. The vapor temperature profile becomes flatter with increasing inlet quality. For the conditions of Fig. 11, the maximum transverse variation in vapor temperature (ΔT_{max}) is reduced from 120 to 40°C when the inlet quality is increased from 0.04 to 0.40. More data were obtained at various inlet qualities and mass fluxes and are shown in Fig. 12. It is seen that the effect of mass flux is similar to the effect of vapor quality; the vapor temperature profile becomes flatter with increasing mass flux. It was also observed that though the vapor temperature profile was influenced by the flow conditions in the channel, the locations of maxima and minima of the vapor temperatures were not affected. The data presented in Figs. 11 and 12 also include several measurements at a given transverse position, and under the same test conditions. Such measurements showed good reproducibility, indicating only 2% scatter in measured superheats (approximately 12°C out of 600°C).

In order to combine the effects of mass flux and the vapor quality on vapor temperature profile, the Reynolds number for the vapor phase (Re_v) is calculated for each measurement point and tabulated in Figs. 11 and 12. The vapor Reynolds number is defined as follows:

$$Re_v = G_v D/\mu_v = x_a GD/\mu_v.$$

The data presented in Figs. 11 and 12 indicate a generally decreasing trend in maximum transverse variation of vapor temperatures, ΔT_{max}, with increasing vapor Reynolds number as shown in Fig. 13.

In order to compare the experimental vapor temperature profiles on a general basis, a non-dimensional form is used in Fig. 14. This figure plots dimensionless vapor temperature, $(T-T_w)/(T_c-T_w)$, vs dimensionless transverse distance, Y/R_0. Also shown in the figure are the predicted non-dimensional temperature profiles for fully developed laminar and turbulent single phase flows under constant wall heat flux [17]. Calculated profiles were based on a pure vapor flowing in a circular duct with a diameter equal to the pitch of the bundle array, shown by $2R_0$ in the figure. It is seen that for low vapor Reynolds numbers (i.e. 1310 and 1398, dark symbols in Fig. 14), the experimental temperature profiles are similar to that encountered in a single phase laminar flow. This implies that the existence of the discontinuous phase (liquid droplets) in the two-phase mixture does not have a noticeable enhancement effect on the heat transfer for such conditions. As the vapor Reynolds number increased (1633–2514), however, the temperature profile started to depart from that of the single phase laminar flow, and agreed better with that of the fully developed single phase turbulent flow. With further increase in Re_v, the non-dimensional temperature profile for the two phases became very flat; implying that the dispersion of liquid droplets increase with increasing Re_v and, in turn, enhance the heat transfer process. It may be concluded from Fig. 14 that, for $Re_v < 1400$ the measured vapor temperature profiles (shown with dark symbols in Fig. 14) are similar to that of fully developed laminar single phase flow. For Re_v values between 1400 and 2600 the vapor temperature profiles are similar to that of fully developed turbulent single phase flow. For Re_v values larger than about 2600 the vapor temperature profiles are almost flat with dimensionless temperature variations of less than 10% for most of the channel.

The above results indicate that the vapor temperatures measured at one fixed transverse position (i.e. the center of the inner cell) in the previous studies [5–9] were the minimum values. These minimum values of vapor temperatures have been used as a bulk vapor temperature for a typical cell in the model development studies. The present results reveal that

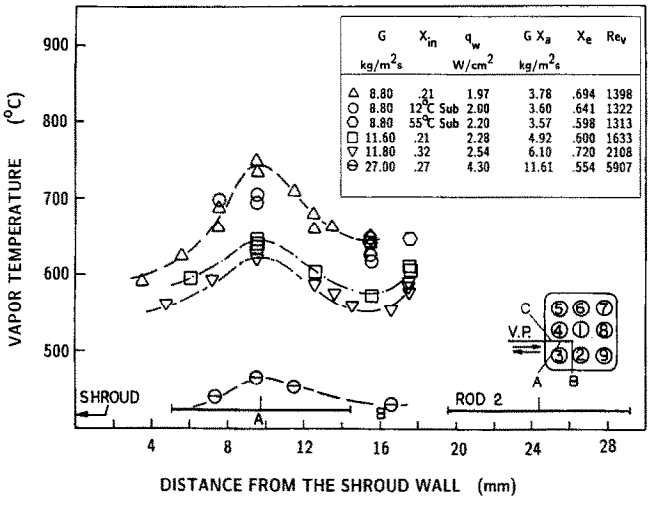

FIG. 12. The effect of mass flux on the transverse vapor temperature profile.

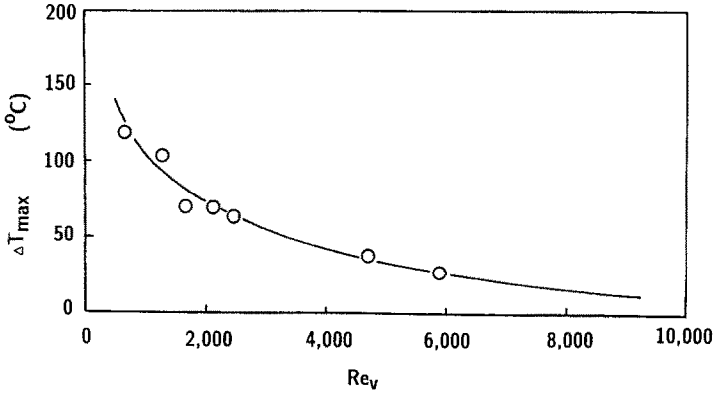

FIG. 13. Variation of maximum temperature difference with Reynolds number.

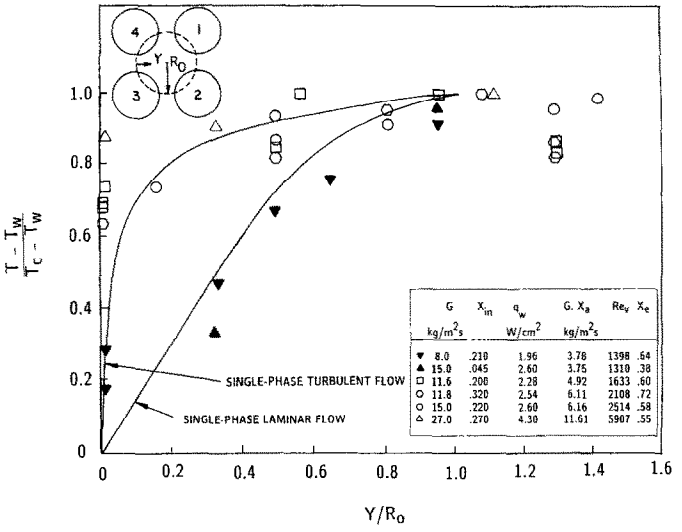

FIG. 14. Comparison of non-dimensional transverse vapor temperature profiles with non-dimensional single phase turbulent and laminar transverse temperature profiles.

the use of cell-centerline vapor temperature as a bulk vapor temperature is only satisfactory for $Re_v > 2600$. For $Re_v < 2600$, the models should consider the transverse variation of the vapor temperature.

The grid spacer effect of vapor temperature profile

The grid spacers are structural members used in the reactor core to support the rod bundle array at the proper rod pitch. The honeycomb grid spacer used in this experiment is one of several types normally found in reactor cores. The grid spacer, being an obstruction in the flow stream, increases the pressure drop, and tends to increase the local heat transfer causing additional evaporation and desuperheating of the wall. Such an enhancement of post-CHF heat transfer around a grid spacer was described by several mechanisms [18]. Irrespective of the mechanism of heat transfer enhancement, the grid spacer seems to have an important effect on vapor temperature. As a result of the desuperheating effect of the spacer, the vapor temperature and its variation in the transverse direction downstream of the grid spacer is expected to be different from the upstream one.

Typical transverse temperature profiles at 203 mm downstream of the grid spacer are presented in Fig. 15 for approximately the same mass flux but different inlet qualities. The figure shows different behavior in the inner and outer cells. In the inner cell, uniform vapor temperature profiles are observed. Such flat temperature profiles would indicate that the presence of the grid spacer causes rearrangement of the size and distribution of liquid droplets and increases the turbulence level in the flow channel. In the outer cell, however, a decrease in vapor temperature is observed as the distance gets closer to the shroud wall. This temperature drop in the outer cell may be attributed to the low temperatures of the shroud walls and the large surface area of the grid spacer in the outer cell relative to the inner cell. Thus, the major finding from this figure is that there is negligible transverse variation of vapor temperature in the inner cell. The above observation could be better illustrated with simultaneous measurements of vapor temperature variation at upstream and downstream locations around the spacer. A typical set of data are presented in Fig. 16. Considering the data in the inner cell, it is seen that the vapor temperature varies about 70°C at the upstream vapor probe location (triangles), while almost a uniform vapor temperature distribution is observed at the downstream vapor probe location (circles). Furthermore, in the absence of a grid spacer, the average vapor temperature would be expected to increase with increasing elevation. In contrast, the figure indicates similar average vapor temperatures for both locations. This is clear evidence of the desuperheating effect of the grid spacer on vapor temperature. While earlier measurements by Chiou *et al.* [16] have indicated that grid spacers tend to desuperheat the wall, the above figure indicates that grid spacers also desuperheat the vapor. To our knowledge, this is the first reported evidence of vapor desuperheating by grid spacers, through simultaneous measurement of vapor temperatures at both sides of a grid spacer.

SUMMARY AND CONCLUSIONS

(1) The hot-patch technique was successfully utilized to stabilize CHF location in a rod bundle, using proportional power control on each rod.

(2) A differentially-aspirated vapor probe of sufficiently small diameter was successfully developed to traverse across the rod bundle for measurement of vapor superheat.

(3) Similar wall superheats for fixed and slowly propagating CHF tests were obtained beyond the length of the hot-patch, under similar operating conditions.

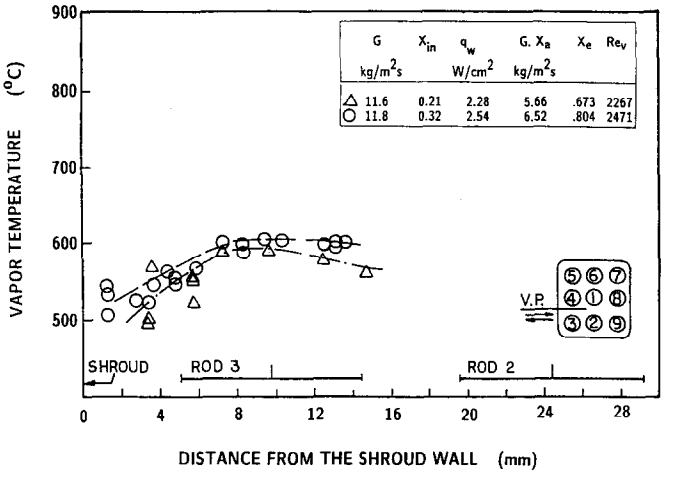

FIG. 15. Typical transverse vapor temperature profiles downstream of the grid spacer.

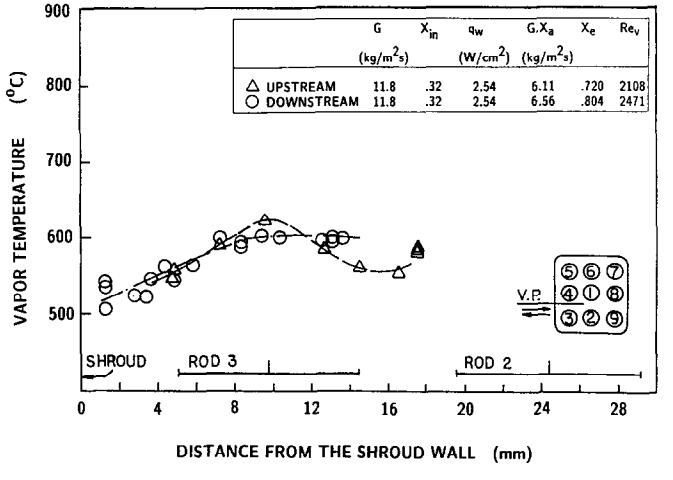

FIG. 16. Comparison of transverse vapor temperature profiles upstream and downstream of the grid spacer.

(4) Significant transverse variations of vapor superheat, up to 120°C, were measured especially at low vapor Reynolds numbers ($Re_v < 1400$). The maximum transverse variation in vapor superheat showed a decreasing trend with increasing vapor Reynolds number. For $Re_v > 2600$, the transverse variation of vapor superheat was found to be insignificant.

(5) Grid spacer reduced the transverse variation of vapor superheat substantially. No significant transverse variation of vapor superheat downstream of the grid spacer was found in the cross-sectional plane of the bundle for operating parameters used in this study.

Acknowledgements—This research was sponsored by the U.S. Nuclear Regulatory Commission under contract No. NRC-04-81-183. The authors acknowledge the continued interest and technical participation provided by Drs Yih-Yun Hsu, Michael Young, Richard Lee and Jose N. Reyes, program managers at USNRC and Dr R. Nelson of LANL, throughout the course of this work.

REFERENCES

1. R. E. Mueller, Film boiling heat transfer measurements in a tubular test section, EURAEC-1971/GEAP-5423 (1967).
2. E. E. Polomik, Transition boiling heat transfer program—final summary report for Feb. 63–Oct. 67, GEAP-5563 (1967).
3. L. E. Hochreiter, NRC/Westinghouse/EPRI FLECHT low flooding rate skew axial profile results, presented at the 5th Water Reactor Safety Information Meeting, Washington, DC (1977).
4. M. J. Loftus, L. E. Hochreiter, C. E. Conway, E. R. Rosal and A. H. Wenzel, Non-equilibrium vapor temperature measurements in rod bundle and steam generator two-phase flows, *Proc. OECD (NEA) CSNI Third Special Meeting on Trans. Two-phase Flow*, Pasadena, California, CSNI Report No. 61 (1981).
5. S. Nijhawan, J. C. Chen, R. K. Sundaram and E. J. London, Measurements of vapor superheat in post-critical-heat-flux boiling, *J. Heat Transfer* **102**, 465–470 (1980).
6. R. C. Gottula, R. A. Nelson, J. C. Chen, S. Neti and R. K. Sundaram, Forced convective nonequilibrium

post-CHF heat transfer experiments in a vertical tube, ASME–JSME Thermal Engng Conf., Honolulu, March (1983).
7. D. Swinnerton, K. G. Pearson and M. L. Hood, Steady state post dryout experiments of low quality and medium pressure, AEEW-R2192, Winfrith (1988).
8. D. G. Evans, S. W. Webb and J. C. Chen, Measurement of axially varying nonequilibrium in post-critical-heat-flux boiling in a vertical tube, *J. Heat Transfer* **107**, 663–669 (1985).
9. C. Unal, K. Tuzla, O. Badr, S. Neti and J. C. Chen, Experimental study of nonequilibrium post-CHF heat transfer in rod bundles, *Proc. Eighth Int. Heat Transfer Conf.*, San Francisco, pp. 2417–2423, August (1980).
10. C. Unal, K. Tuzla, O. Badr, S. Neti and J. C. Chen, Parametric trends for post-CHF heat transfer in rod bundles, *ASME J. Heat Transfer* **110**, 721–727 (August 1988).
11. C. Unal, K. Tuzla, O. Badr, S. Neti and J. Chen, Convective film boiling in a rod bundle: axial variations of evaporation ratio, *Int. J. Heat Mass Transfer* **31**, 2091 (1988).
12. D. C. Groeneveld and S. R. M. Gardiner, A method of obtaining flow film boiling data for subcooled water, *Int. J. Heat Mass Transfer* **21**, 664–665 (1978).
13. C. Unal, An experimental study of thermal non-equilibrium convective boiling in post-critical-heat-flux region in rod bundle, Ph.D. Thesis, Lehigh University, Bethlehem, Pennsylvania (1986).
14. K. Tuzla, C. Unal, O. Badr, S. Neti and J. C. Chen, Thermodynamic nonequilibrium in post-critical-heat-flux boiling in a rod bundle, NUREG/CR-5095, Vols 1–4 (1988).
15. K. Tuzla, C. Unal, O. A. Badr, S. Neti and J. C. Chen, Two-phase 3×3 rod bundle test facility for post-critical heat flux boiling, NUREG/CR-3849 (1984).
16. J. Chiou, L. E. Hochreiter, D. B. Utton and M. Y. Young, Spacer grid heat transfer effect during reflood, ANS/NRC Meeting, Washington, DC, 15 September (1982).
17. W. M. Kays and M. E. Crawford, *Convective Heat and Mass Transfer*, 2nd Edn. McGraw-Hill, New York (1980).
18. S. C. Yao, L. E. Hochreiter and W. J. Leech, Heat transfer augmentation in rod bundles near grid spacer, *Trans ASME, J. Heat Transfer* **104**, 76 (February 1982).

EBULLITION CONVECTIVE DANS UNE GRAPPE DE TUBES: VARIATION TRANSVERSE DE TEMPERATURE DE VAPEUR SURCHAUFFEE DANS DES CONDITIONS STABILISEES POST CHF

Résumé—Les variations transverses de température de vapeur surchauffée dans une nappe de tubes sont mesurées pour l'ébullition convective d'eau dans le régime post CHF. On observe des différences significatives dans la surchauffe (jusqu'à 120°C) à travers les sous-canaux. L'amplitude de ces profils transversaux de surchauffe décroît quand le nombre de Reynolds de la vapeur augmente.

KONVEKTIVES SIEDEN IN EINEM ROHRBÜNDEL: VARIATION DER DAMPFÜBERHITZUNG IN EINEM STRÖMUNGSQUERSCHNITT NACH ÜBERSCHREITEN DER KRITISCHEN WÄRMESTROMDICHTE

Zusammenfassung—Es werden Variationen der Dampfüberhitzung in einem Strömungsquerschnitt eines Rohrbündels beim konvektiven Sieden oberhalb der kritischen Wärmestromdichte gemessen. In einzelnen Unterkanälen der Strömung werden signifikante Unterschiede der Überhitzung (bis zu 120°C) beobachtet. Die Steilheit dieses quergerichteten Überhitzungsprofils nimmt mit steigender Dampf-Reynolds-Zahl ab.

КОНВЕКТИВНОЕ КИПЕНИЕ В СТЕРЖНЕВОМ ПУЧКЕ: ПОПЕРЕЧНОЕ ИЗМЕНЕНИЕ ТЕМПЕРАТУРЫ ПЕРЕГРЕВА ПАРА В УСЛОВИЯХ СТАБИЛИЗИРОВАННОГО ЗАКРИТИЧЕСКОГО ТЕПЛОВОГО ПОТОКА

Аннотация—Измеряются поперечные изменения степени перегрева пара в стержневом пучке при конвективном кипении воды в режиме закритического теплового потока. В ответвлениях течения наблюдаются существенные различия степени перегрева. Крутизна поперечного профиля перегрева уменьшается с ростом числа Рейнольдса для пара.